Journal of Chemical Health Risks

www.jchr.org

JCHR (2023) 13(6), 2569-2588 | ISSN:2251-6727

Pharmacological Evaluation and Characterization of Hyaluronic Acid-Based Hydrogel Embedded with Peptide Nanofibers for Wound Healing

Sheetal Mishra[1],Lalita Sandey[2], Alka Verma[3], Hemlata Sahu[4], Shahbaz Rathor[5], Bharti Gajbe[6], Jhakeshwar Prasad[*7]

[1, 3]Shri Shankaracharya Institute of Pharmaceutical Sciences and Research Junwani – 490020, Bhilai, Chhattisgarh, India
[2]LCIT School of Pharmacy, Bodari, Bilaspur – 495223, Chhattisgarh, India
[4, 5]Kamla Institute of Pharmaceutical Science, Junwani – 490020, Bhilai, Chhattisgarh, India
[6]Shri Rawatpura Sarkar University, Dhaneli, Raipur – 492016, Chhattisgarh, India
[7]Shri Shankaracharya College of Pharmaceutical Sciences, Junwani – 490020, Bhilai, Chhattisgarh, India

***Corresponding author: -** Jhakeshwar Prasad
*Shri Shankaracharya College of Pharmaceutical Sciences, Junwani – 490020, Bhilai, Chhattisgarh, India

KEYWORDS
Hyaluronic acid;
Photo-crosslinking;
Hydrogel;
Wound healing;
GHK peptide;
Peptide nanofibers;
Copper peptide.

ABSTRACT
A versatile hydrogel was developed for enhancing bioactive wound healing by introducing the amphiphilic GHK peptide (GHK-C16) into a photo-crosslinkabletyramine-modified hyaluronic acid (HA-Ty). GHK-C16 self-assembled into GHK nanofibers (GHK NF) in HA-Ty solution, which underwent in situ gelation after the wound area was filled with precursor solution. Blue light irradiation (460–490 nm), with riboflavin phosphate as a photoinitiator, was used to trigger crosslinking, which enhanced the stability of the highly degradable hyaluronic acid and enabled sustained release of the nanostructured GHK derivatives. The hydrogels provided a microenvironment that promoted the proliferation of dermal fibroblasts and the activation of cytokines, leading to reduced inflammation and increased collagen expression during wound healing. The complexation of Cu2+ into GHK nanofibers resulted in superior wound healing capabilities compared with non-lipidated GHK peptide with a comparable level of growth factor (EGF). Additionally, nanostructured Cu-GHK improved angiogenesis through vascular endothelial growth factor (VEGF) activation, which exerted a synergistic therapeutic effect. Furthermore, *in vivo* wound healing experiments revealed that the Cu-GHK NF/HA-Ty hydrogel accelerated wound healing through densely packed remodeled collagen in the dermis and promoting the growth of denser fibroblasts. HA-Ty hydrogels incorporating GHK NF also possessed improved mechanical properties and a faster wound healing rate, making them suitable for advanced bioactive wound healing applications.

1. INTRODUCTION

Wound healing is a complex process that involves the coordination of multiple physiological and cellular processes. There are four steps involved: hemostasis, inflammation, proliferation, and remodeling. [1] This process is regulated by cooperation between various cell types that respond to fundamental treatments, including dermal keratinocytes, fibroblasts, epithelial and endothelial cells, cytokines, and growth factors. Wound dressings are essential for the immediate medical treatment of skin injuries and promoting wound healing. Traditional wound dressings, such as gauzes and bandages, have a limited capability to promote healing and protect against infection. [2] In recent years, there has been growing interest in the development of bioactive wound healing materials, which are designed to enhance the wound healing process and promote tissue regeneration. Bioactive wound healing materials are designed to contain active ingredients such as antimicrobial agents or growth factors; such materials promote healing and reduce the risk of infection. [3] These materials can take various

Journal of Chemical Health Risks

www.jchr.org

JCHR (2023) 13(6), 2569-2588 | ISSN:2251-6727

forms, including hydrogels foams alginates and films and can be tailored to meet the specific needs of different types of wounds. Despite advances in bioactive wound healing materials, there is a continued need for the development of ideal wound healing materials that can effectively and consistently enhance tissue regeneration while also being widely available and cost-effective in various medical settings. [4]

Extensive investigations have been conducted into biopolymer based hydrogels for biomaterials in biomedical applications, including drug delivery cell therapy tissue regeneration and as scaffolds in tissue engineering. [5] This is due to their biocompatibility, anti-inflammatory properties, hydrophilic nature, and biodegradable microstructures that confer multiple functions. Furthermore, these hydrogels offer both a natural extracellular matrix-like environment for wound healing and controlled-release properties that enhance effective drug treatment. Among the various biopolymers, hyaluronic acid (HA) is a major constituent of connective tissues, including the skin. HA plays a critical role in the hygroscopicity and viscoelasticity of the extracellular matrix in the body. In addition, it can reduce inflammation while supporting cell adhesion and collagen expression, which contribute to the wound healing process. [6] More specifically, HA is involved in neovascularization, cell proliferation, cell migration, and tissue organization, and it serves as a signaling molecule that interacts with various receptors to regulate the stimulation of cytokine activity. Despite being an attractive material for biomedical applications, HA has poor stability in the body due to its rapid degradation by reactive oxygen species and hyaluronidase, hindering its long-term stability. [7] Several studies have shown that the stability of HA-based materials can be increased by modifying them through blending with reinforcing materials or crosslinking (enzymatic or photochemical) reactions. To further enhance the bioactivity of HA materials, growth factors and diverse biological molecules can be embedded in the HA materials, thus promoting tissue regeneration in the surrounding area due to sustained release of the active ingredients. However, the embedding of growth factors or other biological molecules in hydrogels may result in high treatment cost or the possibility of uncontrolled side reactions. [8]

The GHK (glycyl-l-histidyl-l-lysine) peptide, a matrikine derived from the extracellular matrix, has shown promising wound healing properties when delivered in the form of a copper complex. GHK can stimulate the production of collagen and glycosaminoglycans along with blood vessel formation,leading to wound contraction. Additionally, GHK can increase the production of growth factors such as vascular endothelial growth factor (VEGF), epidermal growth factor (EGF), basic fibroblast growth factor (bFGF) and cytokines which regulate the wound healing response. [9] This peptide has been reported to exhibit anti-inflammatory and antioxidant properties, aiding in the reduction of oxidative stress and inflammation at the wound site. Consequently, it fosters a more favorable environment for wound healing. Despite the great potential of GHK as a wound healing agent, its limited biochemical stability (half-life <30 min in human serum) poses challenges in terms of preservation and effective delivery to wound sites. As a result, its clinical application remains relatively uncommon. GHK-Cu2+ is known to be rapidly degraded by a weakly acidic environment (such as the skin) or in the presence of peptidases. [10] Therefore, ongoing research is examining methods to improve the stability and delivery of GHK to fully realize its potential as a wound healing agent. Such methods include encapsulating GHK in stable carriers or preserving it within nanostructures. Here, we present a versatile hydrogel, made from photocrosslinkabletyramine-modified HA-Ty and self-assembled GHK nanofibers (GHK NF), with enhanced wound healing properties. GHK-C16, an amphiphilic compound, was utilized to form selfassembled GHK NF within HA-Ty. [11] Through the reduction of electrostatic repulsion among positively charged GHK motifs, GHK-C16 exhibited the ability to self-assemble into nanofibers and effectively integrate into the negatively charged HA-Ty matrix. The release of Cu-GHK nanofibers was shown to stimulate fibroblast proliferation, cytokine activation, and collagen expression, which led to anti-inflammatory effects and improved wound healing, including angiogenesis via VEGF activation. We believe that these hydrogels made from embedding Cu-GHK NF within HA-Ty matrices, exhibit significant promise for advancing bioactive wound healing applications. [12]

Journal of Chemical Health Risks

www.jchr.org

JCHR (2023) 13(6), 2569-2588 | ISSN:2251-6727

2. Experimental methodology

2.1. Materials

Hyaluronic acid (HA, sodium salt, Mw 1200 kDa) was provided by SK Bioland (Bangalore). Fmoc-N-amino acids and 1-hydroxybenzotriazol (HOBt) were purchased from GLbiochem (Mumbai). Rink amide resin was obtained from BeadTech (Mumbai). Copper (II) chloride anhydrous, EDTA disodium salt dehydrate, trifluoroacetic acid (TFA), dichloromethane (DCM), methanol, ethanol, phenol, diethyl ether, and sulfuric acid were purchased from Samchun Pure Chemical Co., Ltd. (Mumbai). *N*,*N*'-diisopropy-lethylamine (DIEA), *N*,*N*'-diisopropylcarbodiimide (DIC), triisopropylsilane (TIPS), thioanisole, 1,2-ethanedithiol, Tween-20, carbazole, sodium tetraborate, hyaluronidase from bovine tests, TentaGelTM S-NH2 and pyrocatechol violet were obtained from Sigma Aldrich (Bangalore). *N*-Methyl-2- pyrrolidone (NMP), acetonitrile (HPLC-grade), and water (HPLCgrade) were purchased from Daejung Chemical Co. (Mumbai). 4-Methylpiperidine and 2× sample buffer (2-mercaptoethanol free, B5834) were purchased from Tokyo Chemical Industry (Mumbai). *N*-(3-Dimethylaminopropyl)-*N*′-ethylcarbodiimide hydrochloride 98% (EDC), *N*-hydroxysulfosuc-cinimide sodium salt, tyramine hydrochloride 99%, and riboflavin 5′-phosphate sodium were purchased from Sigma Aldrich, Co. (Bangalore). Dulbecco's Modified Eagle's Medium (DMEM) and phosphate-buffered saline (PBS) were purchased from Cytiva Life Sciences (Mumbai). Fetal bovine serum was purchased from Atlas biologicals (Gujarat). Transwell® inserts were purchased fromCorning Inc. (Mumbai). The Live/Dead Viability/Cytotoxicity Assay Kit was purchased from Invitrogen (Mumbai). Opti-MEM Reduced Serum Medium and hEGF recombinant Protein (PHG0311L) were purchased from Gibco (Mumbai). PVDF (Polyvinylidene difluoride) membranes were purchased from BIORAD and Thermo Co. (Mumbai). Phospho-Akt (Ser473) (D9E) XP® antibody, Akt (pan) (C67E7) antibody, COL1A1 (E8F4L) XP® antibody, and *β*-Actin antibody were purchased from Cell Signaling Technology (Mumbai). Nrf2 (A-10) antibody, heme oxygenase-1 (A-3) antibody, and VEGF (C-1) antibody were purchased from Santa Cruz Biotechnology (Mumbai).

2.2. Preparation of photo-crosslinked HA-Ty hydrogel

The synthetic method for the tyramine-modified hyaluronic acid (HA-Ty), the GHK peptide, and the GHKC16 (palmitoyl) is provided in the Supplementary Materials. Photo-crosslinked HA-Ty hydrogels were prepared by inducing the formation of di-tyramine through the photo-crosslinking of phenol moieties using riboflavin phosphate and blue light irradiation. HA-Ty (0.5 wt% in deionized water, 1 mL) was mixed with 10 μL of riboflavin 5′-phosphate (10 mg/mL in deionized water) and then exposed to blue light (460–470 nm) at a distance of 15 cm from the hydrogel using a CCP-4 V (Ottawa, Canada) with a light intensity of 5 W/m2 for 5 min. To assess the crosslinking density, we initiated degradation of HA-Ty hydrogels using hyaluronidase (420 mU/mL, 2 mL), and the resulting formation of di-tyramine was subsequently verified using 1H-NMR (700 MHz, D2O)To prepare photo-crosslinked HA-Ty hydrogels containing GHK derivatives, we mixed GHK or GHK-C16 with HA-Ty (0.1 wt%) to form self-assembled nanostructures via electrostatic interaction. When required, copper (II) chloride (0.5 equivalent to GHK derivatives) was introduced to facilitate complexation with the GHK derivatives. Next, we added 100 μL of HA-Ty (0.1 wt%) solution containing GHK derivatives with or without Cu2+ to 900 μL of HA-Ty (0.5 wt%) solution. The process of preparing the photocrosslinked HA-Ty hydrogel embedded with GHK derivatives was the same as previously described.

2.3. Rheological analysis

The storage modulus G' of hydrogels was measured using a constant stress rheometer (HAAKE MARS, Thermo Scientific, USA) equipped with a modular advanced rheometer system at room temperature. Hydrogel samples with or without GHK or GHK-C16 were prepared in CoverWell Perfusion Chambers (Grace Bio-Labs) with a defined shape (diameter, 20 mm; thickness, 1.7 mm). Thefrequency sweep was executed over a range of frequencies spanning from 1 to 100 rad·s-1 at a strain of 1%. This sweep was carried out after identifying the linear viscoelastic region of the storage modulus (G'), where the oscillatory strain changed at a constant frequency.

Journal of Chemical Health Risks

www.jchr.org

JCHR (2023) 13(6), 2569-2588 | ISSN:2251-6727

2.4. Swelling and degradation behavior analysis

Each hydrogel sample, including HA-Ty, GHK/HA-Ty and GHK NF/HA-Ty, was prepared after undergoing 5 min of blue light irradiation within a silicon mold with specified dimensions (1 × 1 × 0.5 cm). To examine the swelling behavior, weight gain measurements were taken for the hydrogel samples. The hydrogel samples were first weighed and then submerged in 3 mL of deionized water at room temperature.

The swelling ratio (S%) of the hydrogel was calculated using the following equation:

Swelling ratio *(*S%*)* = [*(Wt- Wi)/Wi*] × 100

Here, Wt represents the weight of the swollen hydrogel at a specific time point *t* and Wi corresponds to the initial weight of hydrogel. The degradation test examined the released amount of hyaluronic acid using a carbazole assay. [13] Hydrogel samples were subjected to degradation in 4 mL of deionized water containing 100 U of hyaluronidase at 37 °C. For the degradation assay, 100 μL of external solution was taken and replaced with the same volume of fresh solution (Hyaluronidase in deionized water, 25 U/mL). The collected solution was then mixed with 200 μL of 25 mM sodium tetraborate/sulfuric acid solution and heated for 10 min at 100 °C. After cooling to room temperature, 10 μL of 0.125% carbazole solution in ethanol was added, followed by heating to 100 °C for 15 min. Finally, the absorbance of solution at 530 nm was measured using a microplate reader (Synergy H1, Biotek, VT, USA). [14]

2.5. Analysis of the morphology of hydrogels and self-assembled GHK-C16 nanofibers within the hydrogel

After being exposed to blue light for 5 min, the hydrogels underwent a freezing step at -196 °C for 1 min, followed by lyophilization. Following iridium coating at room temperature, the hydrogel's morphology was examined using a field emission scanning electron microscope (FE-SEM, JSM-IT800, NIT Rourkela, Odisha, India) equipped with a secondary electron detector at an accelerating voltage of 15 kV.For the transmission electron microscopy (TEM) analysis of GHK nanofibers, we generated self-assembled GHK-C16 nanofibers in a 0.05 wt% HA-Ty solution. The mixture was vortexed for 30 min at room temperature prior to analysis. A droplet (20 μL) of the GHK-C16 /HA-Ty mixture solution was deposited onto a carboncoated TEM grid that had undergone plasma treatment. The grid was then washed three times using deionized water and subsequently stained with a 2% uranyl acetate solution for a duration of 30 s. The grid was then air-dried for 1 h prior to HR-TEM analysis (JEM ARM 200F, NIT Rourkela, Odisha, India).

2.6. Determination of the critical micelle concentration (CMC)

The N-phenyl-1-naphthylamine (NPN) dye was employed to determine the critical micelle concentration (CMC) of GHK derivatives. The underlying principle of the NPN dye is its minimal fluorescence emission in aqueous environments. however, this changes when it encounters a hydrophobic environment generated by the assembled structure. Then, 10 μL of NPN solution (100 μM in ethanol) was introduced into 1 mL of a 0.1 wt% HA-Ty solution. Dilutions of GHK or GHK-C16 were prepared ranging from 100 mM to 0.195 mM in DMSO. Subsequently, 10 μL of the GHK derivatives solution was blended with 1% NPN within the 0.1 wt% HA-Ty solution. Each resulting mixture (100 μL) was dispensed into wells of a 96-well black plate. Following excitation at 338 nm, fluorescence measurements were taken within the range of 370–550 nm.The critical micelle concentration (CMC) was derived by constructing a plot of the logarithm of GHK derivatives concentrations against the fluorescence signal at 405 nm. Calculation of the CMC involved identifying the point at which the steepest slope intersects the baseline. For the comparison, the CMC of GHK-C16 in deionized water without HA-Ty was also evaluated using the same methodology.

2.7. Copper binding activity of GHK and GHK-C16 peptide

The copper binding characteristics of the GHK peptide derivatives were determined through chelate titration, utilizing pyro-catechol violet (PV) as a metal chelating indicator, following the methodology outlined in a previous report. [15] In this procedure, 200 μL of CuCl2 solution (10 mM in deionized water) was mixed with 100 μL of PV solution (5 mM in deionized water, yellow color) resulting in the formation of a PV-Cu2+

Journal of Chemical Health Risks

www.jchr.org

JCHR (2023) 13(6), 2569-2588 | ISSN:2251-6727

complex with a distinctive blue coloration. Meanwhile, the GHK and GHK-C16 was diluted from 4 mM to 1 mM in deionized water. Subsequently, 10 µL of the GHK derivatives solution was added to 500 µL of 0.1 wt% HA-Ty in HEPES buffer (10 mM, pH 6.0). To investigate color changes resulting from copper chelation by GHK derivatives, the GHK/HA-Ty or GHK-C16/HA-Ty solution was mixed with 6 µL of the PV-Cu2+ complex solution and allowed to incubate for 10 min. If a GHK peptide derivative exhibited Cu2+ binding activity, a yellow coloration emerged as PV released Cu2+ ions. The color change of the PV solution was quantified within 380–850 nm range using a microplate reader. EDTA was used as a positive control for this assessment. [16]

2.8. Cell culture and stimulation

Human dermal fibroblasts (HDFs) cells were cultured in DMEM supplemented with 10% (v/v) fetal bovine serum, 4 mM l-glutamine (Cytiva Co.), sodium pyruvate (Cytiva Co.), and 4500 mg/L of glucose (Cytiva Co.). Cells were maintained in an incubator at 37 °C 5% CO2 in cell culture dishes (90 × 15 mm) and were passaged every 2–3 days (when reaching 90% confluence). To observe the stimulation of GHK or GHK-C16, with or without complexation with Cu2+ ions or EGF, HDF cells were plated at 20,000 cells per well in 6-well plates. On the following day, each well was washed twice with 1× PBS buffer (pH 7.6) and serum-starved with reduced serum Opti-MEM for 24 h in an incubator at 37 °C with 5% of CO2. The cells were then washed twice with 1× PBS and incubated with 2.5 µM GHK or GHK-C16 or 100 ng of EGF, all of which were mixed with 0.05 wt% HA-Ty solution in Opti-MEM for 24 h. Subsequently, the cells were harvested in 2× sample buffer.

2.9. In vitro cell proliferation assay

HDFs were seeded at a density of 10,000 cells per well in 12- well plates. Cells were washed twice with 1× PBS buffer (pH 7.6) and treated with either 2.5 µM GHK or GHK-C16 peptide mixed with 0.05 wt% HA-Ty solution, or 25 µM of GHK or GHK-C16 peptide mixed with 0.5 wt% HA-Ty hydrogels (100 µL) in Transwell® inserts for 24 h at 37 °C with 5% CO2. The next day, HDFs were fixed with 4% paraformaldehyde for 20 min and were then washed three times with 1× PBS buffer at different time points starting from 24 h. The cells were washed twice with distilled water and stained with 0.1% crystal violet for 30 min. After three washes in deionized water, cells were air-dried for 30–60 min at room temperature. Finally, the cells were de-stained with a solution of 10% acetic acid, 50% methanol, and 40% H2O for 15 min, and the optical density at 590 nm was then measured using a microplate reader (BioTek).

2.10. In vitro wound scratch assay

HDF cells were plated at a density of 45,000 cells per well in 24-well plates and allowed to grow to confluency in complete growth medium. The cell monolayer was scratched using a 1000 µL pipette tip, and the cells were washed twice with 1× PBS buffer (pH 7.6) before treatment with either 2.5 µM GHK, GHK-C16 peptide with 0.05 wt% HA-Ty solution or 25 µM GHK, GHK-C16 peptide with 0.5 wt% HA-Ty hydrogels in Transwell inserts. Images of the wound were captured immediately after treatments were applied and then every 24 h to monitor wound closure by cell migration over time. The images were analyzed using ImageJ/FIJI software.

2.11. Western blotting analysis

Cell lysates were separated by SDS-PAGE and transferred onto PVDF (polyvinylidene difluoride) membranes (BIO-RAD and Thermo Co.). Non-specific binding to the membranes was blocked by incubation in 5% skim milk in 1× TBS buffer containing 0.1% Tween-20, and then incubated with the primary antibody at 4 °C overnight. On the next day, the membranes were washed three times in TBS buffer with 0.1% Tween-20 and incubated with the secondary antibody for 90 min at room temperature. The membranes were washed five times (each wash, 5 min) in 1× TBS buffer with 0.1% Tween-20 and then imaged using the Atto Imaging system (WSE-6370 LuminoGraph III Lite).

2.12. Animal studies

Sprague Dawley rats (male, 7 weeks old) were used for *in vivo* full thickness wound healing experiments. Prior to the experiment, all rats were anesthetized with ketamine and xylazine and the dorsal skin was shaved. A wound of 1 cm in diameter was created using a

Journal of Chemical Health Risks

www.jchr.org

JCHR (2023) 13(6), 2569-2588 | ISSN:2251-6727

biopsy puncher on the dorsal side of the skin. The rats were then randomly divided into six groups each containing five rats. The following six groups were established: Group I, untreated Control; Group II, HA-Ty hydrogel; Group III, GHK/HA-Ty hydrogel; Group IV, Cu-GHK/HA-Ty hydrogel; Group V, GHK NF/HA-Ty hydrogel; Group VI, Cu-GHK NF/HA-Ty hydrogel. We dispensed 150 µL of hydrogel precursor solution, containing 0.5 wt% HA-Ty, 25 µM of GHK or GHK-C16 and if necessary 12.5 µM of copper (II) chloride, onto the wound sites using a micropipette to ensure thorough coverage. Subsequently, the precursors solution was carefully spread across the wound surface to guarantee full contact and uniform distribution prior to photo-crosslinking. For photo-crosslinking, the precursor solution within wound was exposed to a LED.D curing light (Woodpecker, China) for 45 s with a light intensity of 650– 850 mW/cm2. Once the *in-situ* hydrogel formation occurred at the wound site, the wound was covered with TegadermTM. The wound size was measured at 0, 3, 7, and 10 days after wounding, and photographs were taken. To ensure the clarity of the wound progression in the images, we captured photographs after carefully removing the initially applied hydrogels. The degree of wound healing was calculated as a percentage of the original wound size. Following the image capture, we promptly applied fresh hydrogels using the same method as the initial application onto the wounds to continue with the experimental process. Mice were sacrificed after 10 days of treatment. One half of the specimen was used for histological analysis and the other half was used for RT-PCR and western blotting. All animal procedures were performed in accordance with the guidelines approved by Institutional Animal Ethics Committee for control and supervision of experiments on animals in India.

2.13. Hematoxylin and eosin (H&E) staining

Deparaffinization of tissue sections was performed in xylene for 30 min, followed by rehydration using a descending ethanol gradient (100%, 90%, and 80%, each for 2 min), and distilled water for 5 min. The samples were immersed in hematoxylin for 5 min and then rinsed in 1× PBS for 3 min to reduce background staining. Next, they were stained with eosin for 2 min and rinsed again in distilled water for 5 min. Dehydration was performed in an increasing ethanol gradient (80%, 90%, 95%, and 100%, each for 5 min), and the final step of clearing was performed in xylene for 15 min. The slides were then mounted with neutral resin and cover-slipped. The stained sections were observed under a light microscope,and epidermal thickness was measured and calculated using ImageJ/FIJI software.

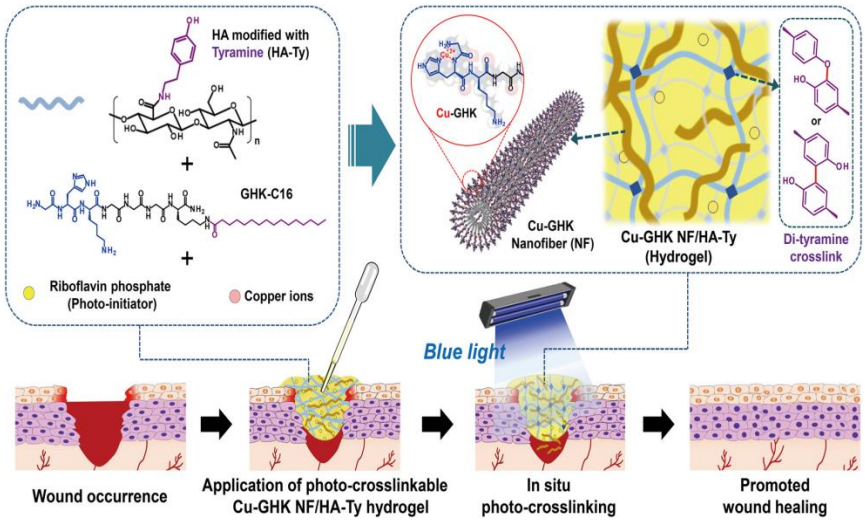

Fig.1. Enhanced skin wound healing using photo-crosslinkable hyaluronic-based hydrogel with self-assembled Cu-GHK-C16 peptide nanofibers (Cu-GHK NF).

Journal of Chemical Health Risks

www.jchr.org

JCHR (2023) 13(6), 2569-2588 | ISSN:2251-6727

2.14. Masson's trichrome staining

The tissue sections underwent deparaffinization and were rehydrated using a decreasing ethanol gradient (100%, 95%, and 70%). Masson's trichrome staining kit was used to stain the sections in accordance with the manufacturer's suggested protocols. Briefly, the cell nuclei were stained with A1:A2 (1:1) for 5 min, and the sections were thoroughly rinsed with water before being submerged in acid alcohol for differentiation for 5 s. Fibrous tissue was stained using Ponceau acid fuchsin solution for 10 min, followed by 1 min in 2% acetic acid solution, 30 s in phosphomolybdic acid solution for differentiation, and 20 s in aniline blue. The sections were then dehydrated, mounted, and cover-slipped as described. The production and intensity of collagen fibers were evaluated using Masson's trichrome stain and quantified using ImageJ/FIJI software.

2.15. Immunofluorescence staining

The tissue sections were deparaffinized three times in xylene solution, each for 5 min, followed by hydration in a decreasing ethanol gradient (100%, 90%, 80%, and 70%, each for 3 min). Non-specific binding sites were blocked by incubating the sections with 4% BSA in 1× PBS at room temperature for 1 h. The blocked sections were then incubated with a primary antibody, κ vimentin antibody (mouse monoclonal IgG1, 1:100, sc-6260, Santa Cruz Biotechnology), diluted in 4% BSA in PBS solution overnight at 4 °C. After three washes (5 min each) in 1× PBS, the sections were incubated with Alexa Flour 488-conjugated secondary antibody (a rabbit anti-mouse IgG, 1:1000, # A-11059, Invitrogen) in the dark for 1 h at room temperature. Nuclear labeling with DAPI and mounting with antifade mounting medium (Invitrogen) followed. Fluorescence signals were then imaged using a confocal microscope (Zeiss LSM 710 or LSM 800, ZEN software, Germany). The intensity of vimentin was analyzed in the images using ImageJ/FIJI software.

2.16. Statistical analysis

All data were obtained from triplicate independent experiments ($n \geq 3$). The results were reported as the mean ± SD (standard deviation). The statistical significance was assessed using one-way ANOVA and denoted as $*p < 0.05$, $**p < 0.01$, and $***p < 0.001$ compared with the control treatment.

3. Results and discussion

3.1. Design and synthesis of photo-crosslinkable HA-Ty and self-assembling GHK-C16

We designed tyramine-modified hyaluronic acid (HA-Ty) based hydrogels with self-assembled GHK peptide nanofibers as the bioactive agent for wound healing applications (Fig. 1). To prepare the HA-Ty hydrogels, we utilized a process in which di-tyramine is formed through the oxidative dimerization of the phenolic groups of tyramine residues. [17] This process was initiated using riboflavin (vitamin B2) phosphate, a naturally occurring photoinitiator under blue light in the range of 460–490 nm. This photocrosslinking process afforded *in situ* gelation of the material when applied in a fluidic state to the skin wound site, resulting in improved mechanical and biochemical stabilities. HA-Ty was synthesized by an *N*-(3-dimethylaminopropyl)-*N*ethylcarbodiimide/*N*-hydroxysuccinimide (EDC/NHS) coupling reaction that activated the carboxylic acid groups of HA (MW: ~1200 kDa) and reacted with tyramine (Fig. S1a). The functionalization of HA with tyramine was confirmed by 1H-NMR analysis, which indicated that approximately 9% of the carboxylic acid groups on HA had been functionalized with a tyramine group (6.5–7.5 ppm, aromatic protons of the conjugated tyramine moieties) [72,73] (Fig. S1b).The bioactive agents, GHK tripeptide and GHK-C16 (palmitoyl)) (Fig. S2and Fig. 3a), were synthesized using a standard Fmoc-based solid-phase peptide synthesis method on the Rink amide resin (loading level: 0.52 mmol/g). The peptides were purified by semi-preparative HPLC (Phenomenex, Torrance, USA) to >95% purity, which was confirmed by ESI–MS analysis (Fig. S2). We then added predetermined amounts of GHK and GHK-C16 to a HA-Ty solution in distilled water (0.5 wt%) to observe their wound healing effect. [18]

Journal of Chemical Health Risks

www.jchr.org

JCHR (2023) 13(6), 2569-2588 | ISSN:2251-6727

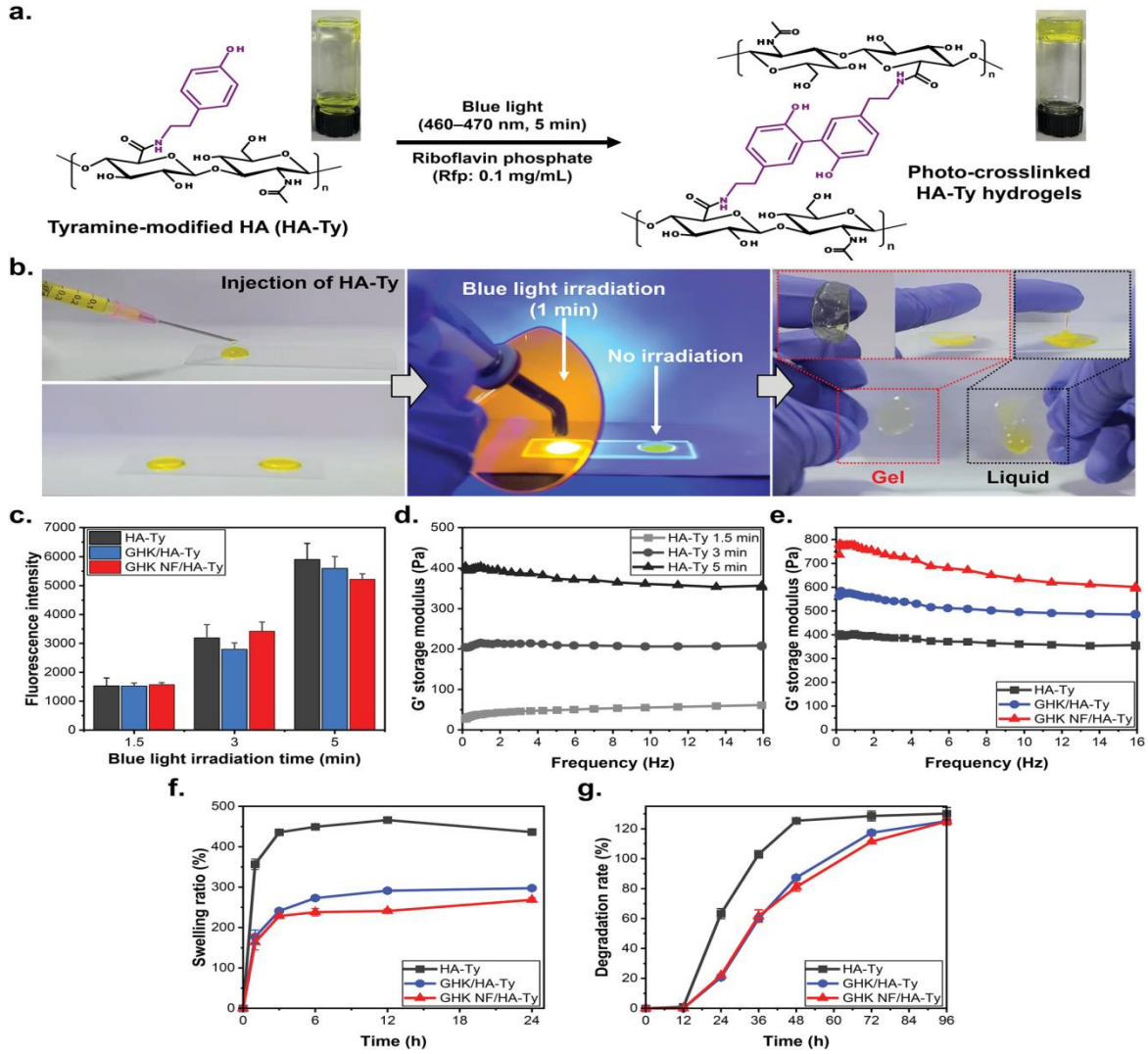

Fig.2. Photo-crosslinking of HA-Ty with GHK derivatives. (a) Schematic representation of the photo-crosslinking process, which involves the formation of di-tyramine using riboflavin phosphate as a photoinitiator. Blue light irradiation (460–470 nm) was applied for 5 min. (b) Photograph showing photo-crosslinking of GHK NF/HA-Ty hydrogel using dental LED.D curing light and the subsequent non-flowing behavior of the hydrogel compared to the precursor liquid before photo-crosslinking. (c) Evaluation of fluorescence intensity as a function of blue light irradiation duration for hydrogel formation. (d) Rheological analysis of 0.5 wt% HA-Ty hydrogels under varying blue light irradiation time: 1.5, 3, and 5 min. (e) Rheological analysis of 0.5 wt% HA-Ty hydrogels, 25 µM of GHK/HA-Ty hydrogels (0.5 wt%) and GHK NF/HA-Ty hydrogels (0.5 wt%) with a frequency dependent storage modulus G′ measurement at 25 °C. (f) Swelling behavior of HA-Ty, GHK/HA-Ty, GHK NF/HA-Ty hydrogels. (g) Degradation assessment of hydrogels in the presence of hyaluronidase. The HA-Ty, GHK/HA-Ty, GHK NF/HA-Ty hydrogels were prepared by 5 min of blue light irradiation.

3.2. Preparation and characterization of photo-crosslinked GHK NF/HA-Ty hydrogels

GHK NF/HA-Ty hydrogels were formulated by crosslinking tyramine-modified HA via riboflavin phosphate-mediated dityramine formation under blue light irradiation. The transformation from a liquid solution to a gel state is visually evident in the images of the inverted container before and after photocrosslinking (Fig. 2a). As shown in Fig. 2b, the preparation process of photo-crosslinked GHK NF/HA-

Journal of Chemical Health Risks

www.jchr.org

JCHR (2023) 13(6), 2569-2588 | ISSN:2251-6727

Ty hydrogel involved injection of precursor solution followed by blue light irradiation, resulting in the sol-gel transition. To assess the gelation time of HA-Ty, a tiltingtest was performed (Fig. S3a). The HA-Ty solution was irradiated under blue light (15 cm) for varying durations, ranging from 1 s to 60 s. With increasing irradiation time, the HA-Ty solution gradually transformed into a gel, requiring a minimum of 50 s when employing a photo-reactor (CCP-4V, Ottawa, Canada). The injectability and photo-crosslinking capability of the hydrogel can be further observed in Movie S1(Supplementary Materials), where the precursor solution solidified upon exposure to blue light using a blue dental curing light (LED.D curing light, Woodpecker, China). The level of di-tyramine generated through photo-crosslinking was assessed by measuring its fluorescence. We assessed the effect of different durations of blue light irradiation (1, 3, and 5 min) on hydrogel formation while maintaining a constant riboflavin concentration (0.1 mg/mL).

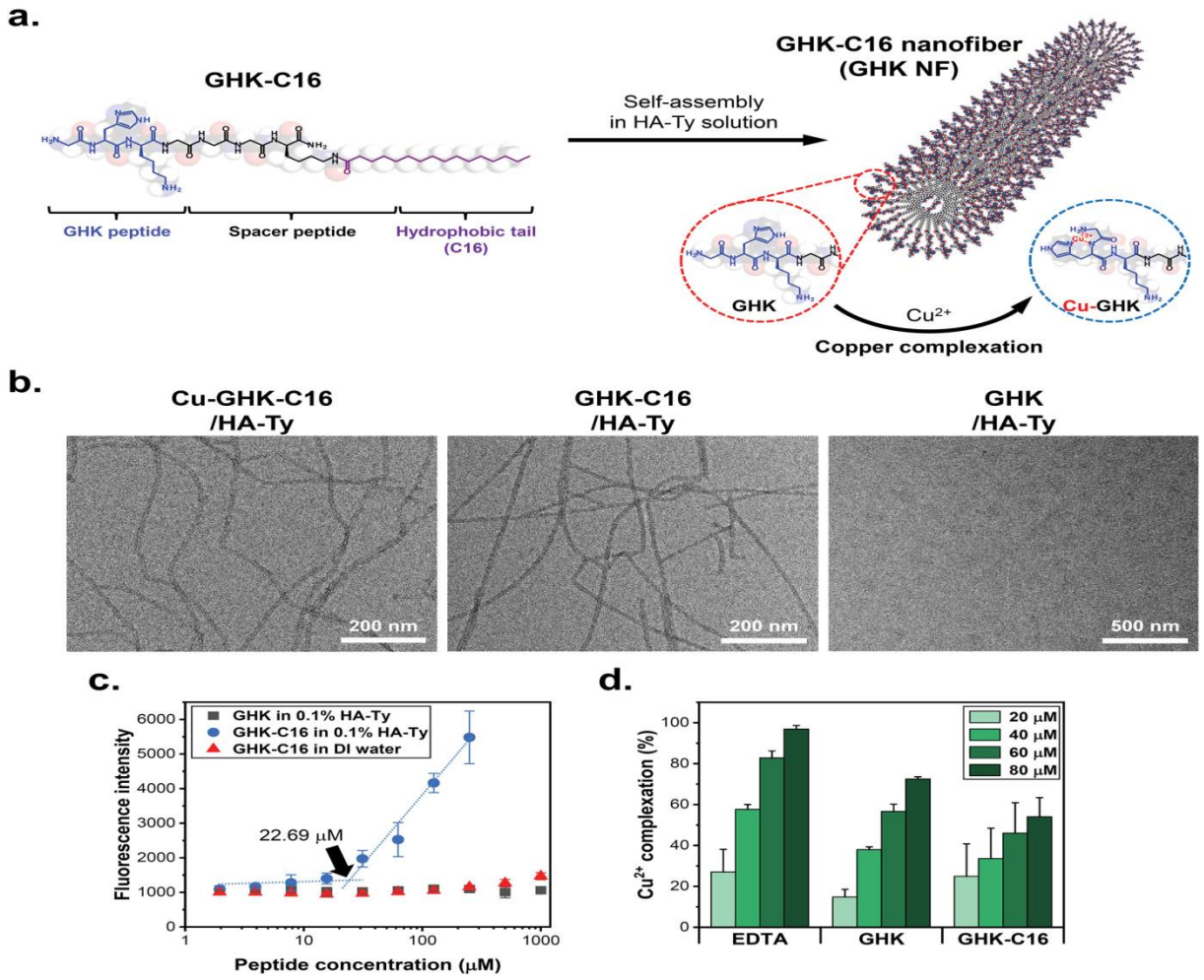

Fig.3. Self-assembly and copper complexation of GHK-C16 with HA-Ty (a) The schematic illustration of self-assembled GHK-C16 nanofiber and copper complexation; composed of GHK peptide, spacer peptide (GGG), and hydrophobic tail. (b) TEM images of the self-assembled Cu-GHK-C16 (left) and GHK-C16 (middle) nanofiber structures in 0.05 wt% HA-Ty solution. GHK in 0.05 wt% HA-Ty solution did not induce nanostructure assembly (right). (c) The determination of critical micelle concentration (CMC) for GHK or GHK-C16 in both 0.1 wt% HA-Ty solution and deionized water (DI water). (d) The copper chelating activity of EDTA, GHK and GHK-C16.

Journal of Chemical Health Risks

www.jchr.org

JCHR (2023) 13(6), 2569-2588 | ISSN:2251-6727

The fluorescence intensity originating from the di-tyramine cross-linking was measured at an emission peak of approximately 400 nm under excitation at 310 nm (Fig. 2c). The fluorescence intensity of the resulting di-tyramine increased with increasing irradiation time (up to 5 min). No significant differences were observed between the hydrogels containing GHK or GHK-C16. We also assessed the di-tyramine formation within the HA-Ty hydrogel using 1H-NMR analysis (Fig. S3b). After subjecting the HA-Ty solution to 5 min of blue light irradiation and subsequently degrading it with hyaluronidase, a reduction in peak intensities corresponding to the aromatic protons on tyramine (depicted as α and β) was observed, suggesting their involvement in the photo-crosslinking reaction. [19] The crosslinking density of HA-Ty hydrogels was determined to be 4% of the tyramine content. The mechanical properties of the hydrogels exhibited a strong correlation with the time-dependent change in fluorescence intensity (Fig. 2d-e). The storage modulus (G') was measured by rheological analysis, indicating the mechanical stiffness of the hydrogel. The G' was determined by applying oscillatory strain at a constant frequency, while the frequency sweep of the hydrogels was performed at frequencies ranging from 1 to 100 rad·s-1 at a strain of 1%. For the HA-Ty hydrogel (0.5 wt%) without any peptide addition, the G' value exhibited a substantial increase, from 42 Pa (1.5 min) to 382.7 Pa (5 min), a ~9-fold increase, as the duration of blue light irradiation was extended (Fig. 2d). This observation underscores that prolonging the blue light irradiation period effectively enhanced the rheological properties of HA-Ty hydrogels. We also performed rheological analysis of HA-Ty hydrogels incorporating GHK derivatives, namely GHK/HA-Ty and GHK NF/HA-Ty, after the pre-mixing GHK derivatives with HA-Ty and subsequent hydrogel formation through 5 min of blue light irradiation. The introduction of GHK and GHK-C16 led to an increase in the G' value of the photo-crosslinked hydrogels compared with the group lacking peptide derivatives (Fig. 2e). [20]

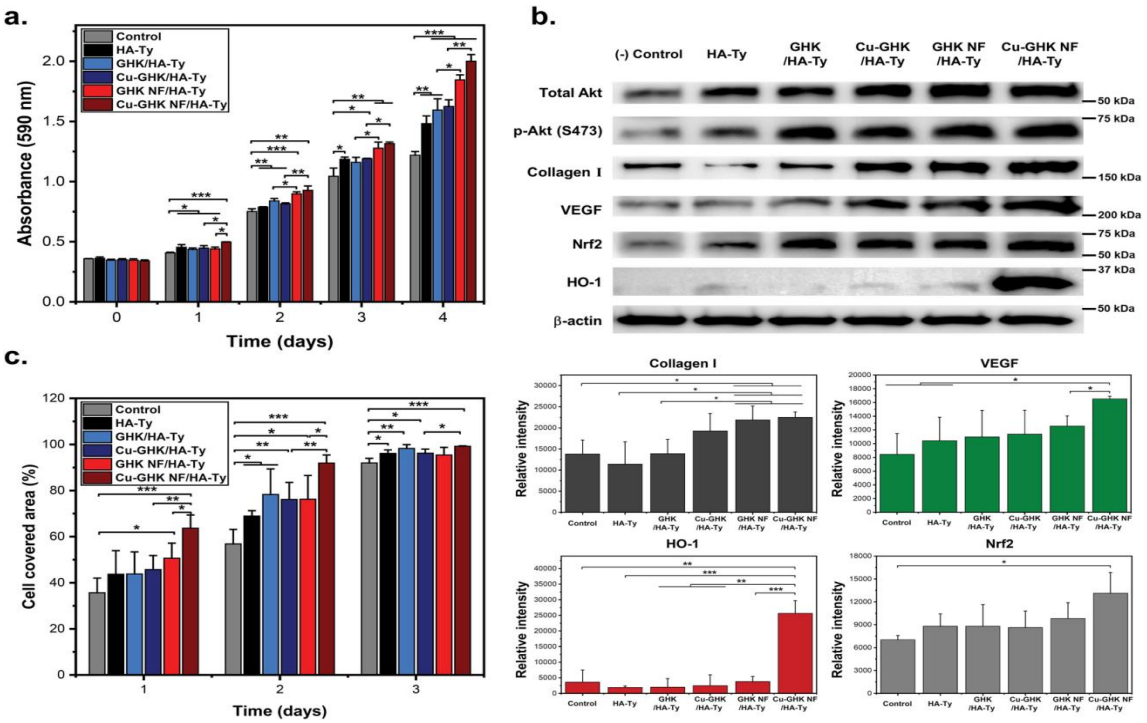

Fig.4. *In vitro* evaluation of the relevance of HA-Ty incorporating GHK derivatives. (a) Cell proliferation assay results for HA-Ty embedded with GHK derivatives. (b) Protein expression validation by western blotting analysis. (c) Analysis of cell migration by the wound scratch assay; HDFs were treated with control, 0.05 wt% HA-Ty solution, 2.5 μM of GHK in 0.05 wt% HA-Ty solution, or GHK-C16 in 0.05 wt% HA-Ty solution with or without Cu2+ ions. ∗p<0.05, ∗∗p <0.01, or ∗∗∗p <0.001.

Journal of Chemical Health Risks

www.jchr.org

JCHR (2023) 13(6), 2569-2588 | ISSN:2251-6727

This result suggests that the GHK peptides contribute to strengthening the hydrogel through electrostatic interactions between two basic residues along with the N-terminal group of GHK and the negatively charged carboxylate-containing HA-Ty hydrogel. Notably, the hydrogels containing self-assembled GHK-C16 exhibited higher stiffness, presumably due to the presence of multivalent cationic GHK groups on the self-assembled nanostructures, which enhanced these electrostatic interactions. Similar trends were observed in the swelling properties of the hydrogels (Fig. 2f). The extent of swelling of hydrogels is inversely related to their crosslinking density. As expected, HA-Ty hydrogel, which exhibited the lowest mechanical stiffness, showed the highest swelling ratio (436.3%). In comparison to GHK/HA-Ty and GHK NF/HA-Ty hydrogels, the swelling ratio of HA-Ty hydrogel was 1.47- and 1.62-fold higher, respectively. The degradation test results exhibited patterns consistent with the swelling behavior of the hydrogels. Whereas the HA-Ty hydrogel completely degraded within 48 h, the degradation rates of HA-Ty hydrogels embedded with GHK derivatives were extended to 96 h (Fig. 2g). Notably, the degradation of the HA-Ty hydrogel coincided with the release of GHK, indicating the potential for sustained release of GHK derivatives.

3.3. Self-assembly of GHK-C16 in HA-Ty, copper complexation, and cytotoxicity

The previously reported self-assembled nanostructure of positively charged peptide amphiphile (PA) with hyaluronic acid (HA), an anionic biopolymer, [21] motivated our exploration of the structural features of GHK-C16 self-assembly within HA-Ty hydrogels using TEM analysis. We found that GHK-C16 adopted selfassemblednanofibrous morphology within the HA-Ty solution (Fig. 3b, middle). In contrast, unmodified GHK did not exhibit any discernible self-assembled structures (Fig. 3b, right). Furthermore, the addition of copper to GHK nanofibers within HA-Ty to create Cu-GHK nanofibers did not alter their morphology (Fig. 3b, left). Subsequently, we assessed the self-assembly behavior of GHKC16 within HA-Ty by determining the critical micelle concentration (CMC) using fluorescent probe, N-phenyl-1-naphthylamine (NPN). As the GHK-C16 concentration increased in the 0.1 wt% HA-Ty solution, the NPN fluorescence intensity also increased, indicating the formation of a self-assembled nanostructure based on the formation of hydrophobic core (Fig. 3c). Notably, based on the NPN fluorescence intensity, only GHK-C16 in the HA-Ty solution exhibited a substantial change in fluorescence, in contrast to both GHK peptide and GHK-C16 in deionized water. This observation suggests that GHK-C16 has the capacity for self-assembly into nanofibers, driven not solely by the hydrophobic palmitoyl tail of the peptide amphiphile but also by the electrostatic screening facilitated by the positively charged GHK head interacting with the negatively charged hyaluronic acid molecules. GHK-C16 exhibited a CMC value of 22.69 μM in the 0.1 wt% HA-Ty solution, while the others exhibited no such self-assembly behavior. [22] The alterations in viscosity within the HA-Ty solution during self-assembly are perceptible to the naked eye.Furthermore, the analysis of circular dichroism (CD) spectroscopy for GHK-C16 in the 0.1 wt% of HA-Ty solution revealed the presence of a random coil configuration with no discernible formation of secondary structures among adjacent peptides (Fig. S4). This observation highlights the essential role of electrostatic inter-actions between the positively charged peptide head and the anionic HA-Ty, rather than secondary structure formation among the peptides, in facilitating the self-assembly into peptide nanofibers. Scanning electron microscopy (SEM) analysis indicated that the morphology of the 0.5 wt% HA-Ty hydrogel, photo-crosslinked for 5 min, remained mainly unchanged regardless of whether it contained 25 μM GHK or 25 μM GHK-C16 (Fig. S5).

Journal of Chemical Health Risks

www.jchr.org

JCHR (2023) 13(6), 2569-2588 | ISSN:2251-6727

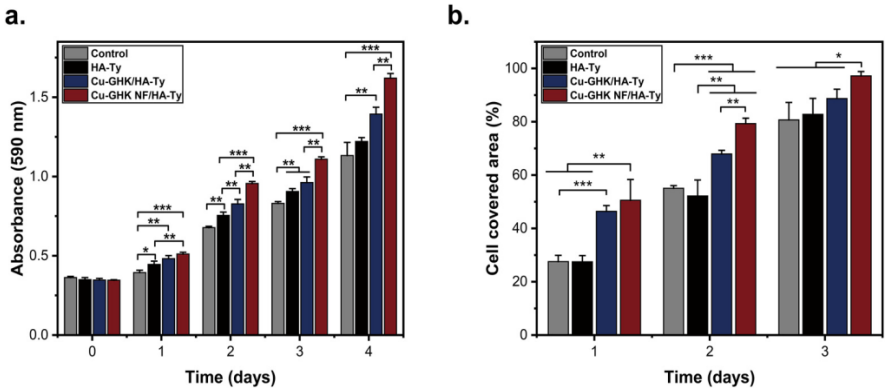

Fig.5. *In-vitro* evaluation of the relevance of photo-crosslinked HA-Ty hydrogels incorporating GHK derivatives for wound healing. (a) Results of HDF proliferation assay over a 4-days period. (b) HDF migration analysis using the wound scratch assay. HDFs were subjected to various treatments including the control, 0.5 wt% HA-Ty hydrogel, 25 µM of Cu-GHK in 0.5 wt% HA-Ty hydrogel (Cu-GHK/HA-Ty), and Cu-GHK-C16 in 0.5 wt% HA-Ty hydrogel (Cu-GHK NF/HA-Ty) using Transwell inserts. ∗p<0.05, ∗∗p <0.01, and ∗∗∗p <0.001

The GHK peptide, well known as a copper peptide, exhibited a strong affinity for copper ions. The Cu-GHK complex demonstrated a range of synergistic biological activities. To investigate the complexation of both GHK and GHK-C16 with copper ions, we employed pyrocatechol violet (PV) as an indicator for metal ion binding. [23] As the concentration of EDTA increased, the solution's color shifted dramatically from blue to yellow, which was attributed to the sequestration of Cu2+ ions by EDTA. While both peptides exhibited lower efficiency compared to EDTA, GHK and GHK-C16 demonstrated copper ion chelation activities of 73% and 54%, respectively (Fig. 3d and Fig. S6a-c). The binding of GHK derivatives to copper ions was also confirmed by inductively coupled plasma-mass spectrometry (ICP-MS) with solid-phase GHK or GHK-C16 resins. Upon interaction with copper ions, the color of both GHK and GHK-C16 resins changed to blue, indicating complexation of GHK or GHK-C16 resins with Cu2+ (Fig. S6d). The Cu2+ complexation efficiency for both GHK and GHK-C16 resins was approximately 60%, consistent with the results observed through the PV-based assay (Fig. S6e). Therefore, it is evident that the GHK peptide possesses copper-binding capabilities, which remain functional even in its lipidated form, GHK-C16.When incorporated into a 0.5 wt% photo-crosslinked HA-Ty hydrogel, neither GHK nor GHK-C16 induced significant cytotoxicity in human dermal fibroblasts (HDFs) within the concentration range of 5–25 µM whether complexed with Cu2+ ions or not (Fig. S7a). Additionally, when GHK and GHK-C16 were utilized at concentrations ranging from 0.1 to 10 µM without HA-Ty, no cytotoxic effects were observed (Fig. S7b), indicating that these compounds do not have a detrimental impact on cell viability. [24]

3.4. In vitro study of Cu-GHK-C16 in HA-Ty as wound healing: promoting collagen I remodeling and angiogenesis stimulation in HDFs

Several studies have highlighted the pivotal role of Cu-GHK in activating connective tissue remodeling, including skin tissues. This involved boosting collagen production, stimulating angiogenesis, and mitigating inflammation. These features indicate that Cu-GHK holds promise as an alternative or adjunct therapy to growth factors in wound healing. Nevertheless, a challenge in utilizing Cu-GHK for wound healing is its inherent instability within the body, potentially leading to rapid degradation and decreased efficacy. [25] To overcome these challenges, we employed the amphiphilic GHK peptide (GHK-C16), which self-assembles into nanofibers upon contact with HA-Ty. Such peptide-based nanostructures have demonstrated higher resistance to enzymatic degradation and enhanced interactions with target cells thereby improving the stability and bioactivity of the functional peptide. We treated human dermal fibroblasts (HDFs) with 2.5 µM of GHK, Cu-GHK, GHK-C16, or Cu-GHK-C16 in a 0.05 wt% HA-Ty solution in deionized

Journal of Chemical Health Risks

www.jchr.org

JCHR (2023) 13(6), 2569-2588 | ISSN:2251-6727

water for 4 days to investigate the role of derivatives of GHK and the lipidated form (GHK-C16) in cell growth, migration, and protein expression. Subsequently, we performed cell proliferation assays, scratch assays, and western blotting. Treatment with Cu-GHK-C16/HA-Ty induced a significantly accelerated cell proliferation compared to the control or the GHK/HA-Ty treatment group (Fig. 4a).

This enhancement in proliferation by CuGHK-C16 was consistently observed across various experimental conditions, even within photo-crosslinked hydrogel systems (Fig. 5a). Notably, HA-Ty hydrogels incorporating Cu-GHK-C16 resulted in a significant increase in cell proliferation rate between days 2–4 compared with the control group and the hydrogels incorporating Cu-GHK. Lipidated GHK has been reported to exhibit enhanced membrane permeability [26], and its nanofiber assemblies facilitate more efficient interactions with cells, thereby promoting cell signaling and proliferation, in line with observations made with other peptide. Consequently, it was expected that the release of Cu-GHK-C16 from the HA-Ty hydrogel can lead to greater cell proliferation.We subsequently employed western blotting to investigate the effects of GHK-C16 on the expression of proteins associated with wound healing in HDFs. [27] The phosphatidylinositol 3 kinase (PI3K)/AKT signaling pathway plays a crucial role in various cellular processes, including apoptosis, cell proliferation, the cell cycle, protein synthesis, glucose metabolism, and telomere activity. Moreover, wound healing is closely linked to the PI3K/AKT signaling pathway, as growth factors stimulate anti-inflammatory, proliferative, and migratory responses through its activation. Our western blotting results revealed that all GHK derivatives led to upregulation of phospho-Akt expression (Fig. 4b, p-Akt (S473)). In addition, we conducted western blotting to assess the expression of collagen I and VEGF in HDFs to demonstrate the potential for synergetic therapeutic effects and to elucidate the mechanismof Cu-GHK-C16/HA-Ty in wound repair (Fig. 4b). Collagen I, the main component of the extracellular matrix (ECM) in skin tissue [28], plays a crucial role in ECM formation during the wound healing process. It achieves this by promoting cellular proliferation, facilitating migration, and differentiation. Therefore, an increase in the expression of collagen I serves as an indicator to investigate the role and mechanism of self-assembled GHKC16 in the wound repair process. [29]

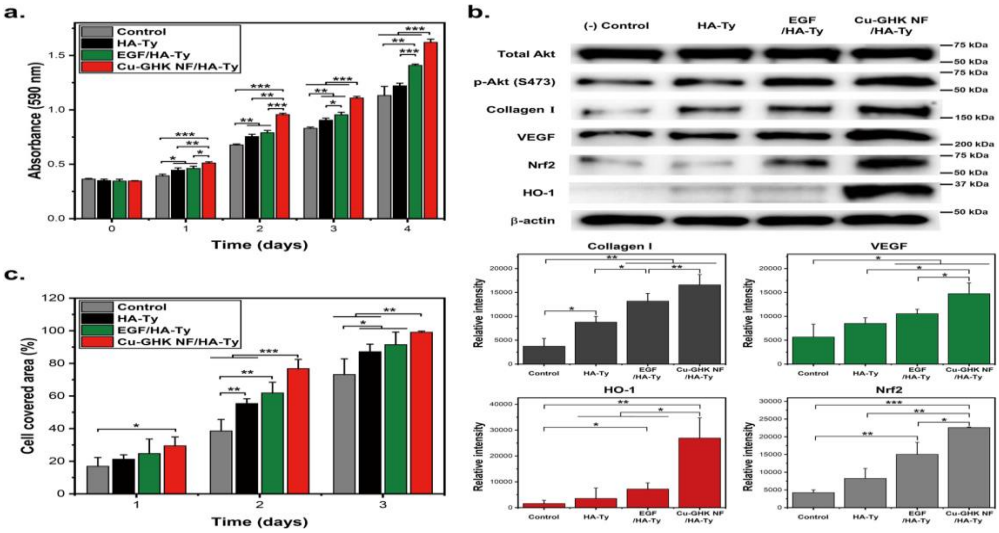

Fig.6. *In vitro* evaluation of Cu-GHK NF/HA-Ty hydrogel and EGF/HA-Ty hydrogel in wound healing. (a) HDF proliferation assay results over a 4-day period. (b) Validation of protein expression following one day of treatment with various hydrogels through western blotting analysis. (c) HDF migration analysis by wound scratch assay; HDFs were treated with control, HA-Ty hydrogel only, 100 ng of EGF in HA-Ty hydrogel (EGF/HA-Ty), and 25 μM of Cu-GHK-C16 in HA-Ty hydrogel (Cu-GHK NF/HA-Ty) using Transwell inserts. *p<0.05, **p <0.01, or ***p <0.001.

Journal of Chemical Health Risks

www.jchr.org

JCHR (2023) 13(6), 2569-2588 | ISSN:2251-6727

The treatment with GHK-C16 nanofibers or Cu-GHK-C16 nanofibers in HA-Ty (0.05 wt%) resulted in significantly higher expression of collagen I compared to both the negative control and the HA-Ty only group (p <0.05), with increases of at least 1.8-fold and 2.7-fold, respectively. Notably, the collagen I levels were even higher in the GHK-C16 and Cu-GHKC16 groups than in the GHK group (p <0.05). VEGF is recognized for its ability to promote wound healing by enhancing collagen remodeling, neovascularization, and epithelialization. [30] Our results revealed a distinct increase in the expression of VEGF after one day of Cu-GHK-C16 treatment relative to both the negative control and the HA-Ty only group (p <0.05), with increases of 1.9- fold and 1.5-fold, respectively. In the Cu-GHK-C16 treatment group, where a complex was formed with Cu2+, the expression level of VEGF surpassed that of the GHK-C16 group, where no complex with Cu2+ was formed. This suggests that the copper complexation process enhances the activity of GHK nanofibers in stimulating VEGF expression. Our findings strongly suggest that Cu-GHKC16/HA-Ty holds immense promise as a highly effective material for promoting wound healing due to its capacity to enhance cellular proliferation, facilitate collagen remodeling, and stimulate angiogenesis. [31]

3.5. Anti-inflammatory effects and enhanced cell migration

GHK has been reported to activate the nuclear factor erythroid 2-related factor 2 (Nrf2) signaling pathways known for their ability to revitalize cellular and molecular mechanisms in wound repair and regeneration. [32] In our study, the GHK and GHKC16 treatment groups with or without Cu2+ ions showed enhanced activation of the Nrf2 pathway (Fig. 4b, Nrf2). Significantly, treatment with Cu-GHK-C16/HA-Ty was found to markedly increase the expression of heme oxygenase-1 (HO-1), a pivotal protein in the wound healing process. HO-1 plays essential roles in antioxidant defense, anti-inflammatory responses, and angiogenesis, all orchestrated through the activated Nrf2 signaling pathway. Conversely, the other treatment groups, including GHK-C16/HA-Ty, Cu-GHK/HA-Ty, and HA-Ty only treatments, exhibited no significant enhancement of HO-1 expression. These results suggest that the integration of Cu-GHK-C16 nanofibers into HA-Ty represents a promising therapeutic approach for wound repair due to its ability to reduce oxidative stress and inflammation, and to promote tissue regeneration using the nanostructured bioactive copper peptide. [33-35]

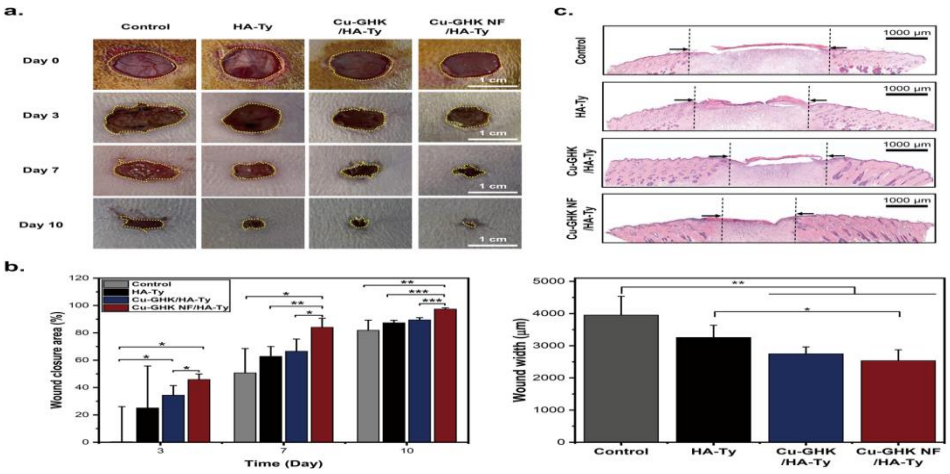

Fig.7. Acceleration of wound healing in rat by applying HA-Ty hydrogels containing self-assembled Cu-GHK-C16. (a) Representative images of the wound areas on days 0, 3, 7, and 10 for the following groups: untreated control, HA-Ty hydrogel only, Cu-GHK/HA-Ty hydrogel, Cu-GHK NF/HA-Ty hydrogel. (b) Measurement of the wound closure at the specified time intervals. (c) Representative images of H&E-stained wound sites taken on day 10 for the following groups: untreated control, HA-Ty hydrogel only, Cu-GHK/HA-Ty hydrogel, Cu-GHK NF/HA-Ty hydrogel. *p<0.05, **p <0.01 or ***p <0.001

Journal of Chemical Health Risks

www.jchr.org

JCHR (2023) 13(6), 2569-2588 | ISSN:2251-6727

To gain further insights into this wound repair effect, we conducted *in vitro* scratch wound healing assays using human dermal fibroblasts. We simulated and observed wound closure for three days after treating the scratched cellular monolayer with HA-Ty or Cu-GHK/HA-Ty, or Cu-GHK-C16/HA-Ty solution (0.05 wt%). As shown in Fig. 4C and Figure S8, cell migration was enhanced in all cases compared to the control. Remarkably, the Cu-GHK-C16/HATy exhibited faster cell migration than Cu-GHK/HA-Ty during days 1–2, and this trend persisted for the entire three-day duration. This enhanced efficacy can be attributed to the improved stability and enhanced bioactivity of nanostructured Cu-GHK-C16 during the scratch repair process. Similarly, cell migration studies using the photo-crosslinked 0.5 wt% HA-Ty hydrogel system in Transwell inserts yielded results consistent with those using the HA-Ty solution (Fig. 5b and Fig. S9). Notably, the migration of cells treated with Cu-GHK NF/HA-Ty hydrogels significantly increased on days 1–2 compared to the control group. These findings also suggest the significant potential of nanostructured Cu-GHK NF within a HA-Ty hydrogel as a therapeutic agent for wound healing applications.

3.6. Self-assembled Cu-GHK NF as a potential alternative to conventional growth factors

To assess the potential of self-assembled Cu-GHK NF as a substitute for conventional growth factors, we conducted a comparative analysis of its effectiveness alongside epidermal growth factor (EGF) within our HA-Ty hydrogel systems. While growth factors such as EGF, VEGF, basic fibroblast growth factor (bFGF), and transforming growth factor beta 1 (TGF-β1) play a crucial role in wound healing by promoting cell proliferation and migration [36] through cytokines and signaling pathways, they come with limitations related to stability rapid diffusion potential unknown inflammatory side effects and cost-effectiveness. In contrast, our self-assembled Cu-GHK NF in HA-Ty offers an innovative approach to wound healing. As shown in Fig. 6a and Figure S10, Cu-GHK NF exhibits potential as a potent bionanomaterial that enhances wound healing by promoting 15% greater cell proliferation and improved wound coverage compared to EGFcontaining HA-Ty hydrogels. Additionally, the expression levels of collagen I were 4.4- and 1.9-fold higher than in the untreated control and HA-Ty only groups (p <0.01) and approximately 20% (1.2-fold) higher than EGF-containing HA-Ty hydrogels (p <0.01). We also performed a quantitative analysis of the angiogenesispromoting effect of Cu-GHK NF/HA-Ty hydrogel by analyzing VEGF expression (Fig. 6b), which was 2.6- and 1.7-fold higher relative to the untreated control and HA-Ty only groups, and 1.4-fold higher than EGF-containing in HA-Ty hydrogels (p <0.05). Furthermore, Cu-GHK NF/HA-Ty hydrogel induced a significant upregulation of HO-1 expression, known for its anti-inflammatory effects and influence on collagen I remodeling. Specifically, the Cu-GHK NF/HATy hydrogel exhibited a 90% increase in HO-1 expression relative to the control and EGF-containing HA-Ty hydrogel groups (Fig. 6b, p <0.01 and p <0.05). Consequently, our findings demonstrate that the self-assembled Cu-GHK NF delivered within the HA-Ty hydrogel presents itself as a potent biomaterial for wound healing. [37, 38] This is attributed to the elevated levels of HO-1 expression, collagen I, and VEGF expression in comparison to EGF-containing HA-Ty hydrogels. Furthermore, we confirmed that the Cu-GHK NF/HA-Ty hydrogel achieved approximately 17% faster scratch coverage than the EGF-containing HA-Ty hydrogel when employed in Transwell inserts (Fig. 6**c**). This result indicates that the combination of CuGHK NF with HA-Ty hydrogel systems holds substantial potential as an effective alternative to conventional growth factors in the treatment of wounds. [39, 40]

Journal of Chemical Health Risks

www.jchr.org

JCHR (2023) 13(6), 2569-2588 | ISSN:2251-6727

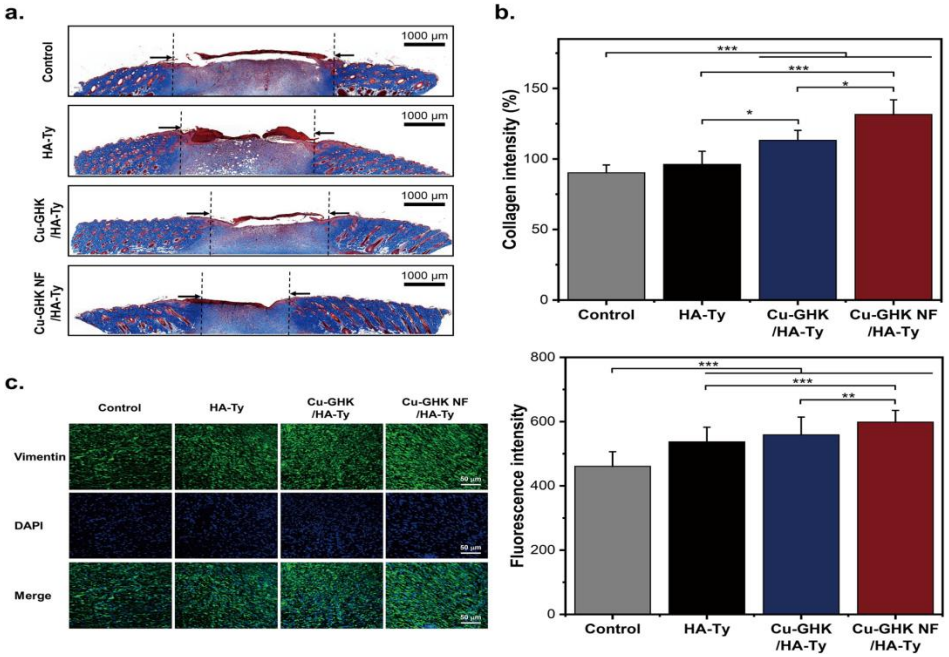

Fig.8. Wound tissue analysis after *in vivo* treatment with hydrogels. (a) Representative images of Masson's trichrome-stained tissue sections of wounds treated with HA-Ty only, Cu-GHK/HA-Ty hydrogel and Cu-GHK NF/HA-Ty hydrogel on day 10 (blue = collagen; red = cytoplasm and muscle fibers). (b) Analysis of collagen intensity compared to the control group. (c) Representative immunofluorescence staining of vimentin in wound sites for the following groups on day 10: untreated control, HA-Ty hydrogel only, Cu-GHK/HA-Ty hydrogel, Cu-GHKNF/HA-Ty hydrogel. The graph (right) shows the quantification of the average fluorescence intensity of vimentin. *p<0.05, **p <0.01, or ***p <0.001. (For interpretation of the references to color in this figure legend, the reader is referred to the web version of this article.)

3.7. In vivo wound healing experiments

A series of experiments was conducted using a rat model to evaluate the *in vivo* wound healing potential of our Cu-GHK NF/HA-Ty hydrogel for skin wounds. Wound incisions of 1 cm were made through the full thickness of the dorsal skin of anesthetized rats (male, 7 weeks old). The treatments applied included HATy hydrogel, Cu-GHK/HA-Ty hydrogel, Cu-GHK NF/HA-Ty hydrogel, and a negative control. The wound healing process following threetreatments on days 0, 3, and 7 is visualized in Fig. 7a. Generally, a healing response was observed in all experimental groups without any adverse effects, except for the negative control group, which exhibited an inflammatory reaction in the wound area on Day 3. We also performed a quantitative analysis of the wound size at predetermined time points (Fig. 7b). The untreated control group displayed the slowest wound healing after 10 days, with an unhealed wound area accounting for 16.4% compared to the initial wound size. On day 3, the Cu-GHK NF/HA-Ty hydrogel group demonstrated the fastest initial wound covering rate at 43%. By day 7, the Cu-GHK NF/HA-Ty hydrogel group exhibited the most substantial wound closure area, reaching 83%, in comparison to the HA-Ty only (62%) and Cu-GHK/HA-Ty hydrogel (64%) groups. Among the various treatments, the Cu-GHK NF/HA-Ty hydrogel group showed the most rapid and effective healing over the 10- day period, achieving nearly complete closure of the wound area (97%). To evaluate the wound repair potential of the Cu-GHK NF/HA-Ty hydrogel, we performed histological analysis of wound tissue sections using hematoxylin and eosin (H&E) staining after 10 days of treatment. The results revealed that the Cu-GHK NF/HA-Ty hydrogel promoted densely packed tissue regeneration (Fig. 7c) although all treatment groups showed potential recovery of the epidermal layer and wound

Journal of Chemical Health Risks

www.jchr.org

JCHR (2023) 13(6), 2569-2588 | ISSN:2251-6727

closure. Additionally, Masson's trichrome staining demonstrated more pronounced staining of remodeled collagen in the dermis of wound areas treated with Cu-GHK/HA-Ty and Cu-GHK NF/HA-Ty hydrogels compared to those treated with HATy hydrogel without peptide derivatives and the negative control. This indicated significant collagen remodeling in the wound area treated with Cu-GHK NF/HA-Ty (Fig. 8a).

We quantified the intensity of blue-stained remodeled collagen in the wound area after each treatment and observed that the Cu-GHK NF/HA-Ty hydrogel upregulated collagen remodeling by 31.4%, 26.8%, and 13.9% compared to the untreated control, HA-Ty hydrogel only, and CuGHK/HA-Ty hydrogel, respectively, after 10 days (Fig. 8b). Furthermore, we conducted vimentin staining to assess fibroblast cell density in the wound tissue after 10 days of treatment. The Cu-GHK NF/HA-Ty hydrogel yielded a higher density of fibroblasts, which was evident from the stronger staining intensity when compared to the other treatment groups (Fig. 8c). Additionally, we investigated the effectiveness of the Cu-GHK NF/HA-Ty hydrogel after its application to the wound site through western blot and RT-PCR analysis (Fig. S11). The protein expression levels increased following hydrogel application (Fig. S11a). Treatments with the Cu-GHK NF/HA-Ty hydrogel led to significantly higher expression levels of collagen I and VEGF compared to the negative control, with increases of 1.7- and 1.5-fold, respectively. This trend was mirrored in the mRNA levels of collagen I, VEGF, and HO-1 (Fig. S11b). In accordance with RT-PCR analysis, the CuGHK NF/HA-Ty hydrogel group enhanced the wound healing process by simulating mRNA expression. Based on these findings, we conclude that the Cu-GHK NF/HA-Ty hydrogel represents a highly effective wound healing material.

4. Conclusions

In this study, we developed a versatile hydrogel with promising applications in wound healing. This hydrogel combines photo-crosslinkabletyramine-modified hyaluronic acid with selfassembled GHK-C16 peptide nanofibers (NF). Our findings highlight that the Cu-GHK NF/HA-Ty hydrogel's considerable advantages as a wound healing material, including its ability to enhance cell proliferation, migration, and collagen remodeling. Importantly, we observed that GHK-C16 peptide nanofibers in the HA-Ty hydrogel exhibited potent anti-inflammatory effects when complexed with copper ions (Cu-GHK-C16). These beneficial effects can be attributed to the unique properties of self-assembled GHK-C16 peptide nanofibers in the HA-Ty hydrogel system. They both stimulate cytokine activation and support robust collagen remodeling and enhance angiogenesis during the wound healing process. Our study suggests that incorporating self-assembled GHK nanofibers into HA-Ty holds significant promise for therapeutic applications, offering a cost-effective and efficient alternative to expensive growth factors. Furthermore, the *in-situ* photocrosslinkable nature of these hydrogels allows for easy customization to match the wound shape through blue light irradiation in combination with the natural photoinitiator riboflavin phosphate. *In vivo* wound healing experiments also revealed that the Cu-GHK NF/HA-Ty hydrogel significantly promoted wound healing; resulting in almost complete closure of the wound area, as indicated by densely packed regenerated tissue, collagen remodeling in the dermis, and more densely packed fibroblasts after treatment. Thus, the Cu-GHK NF/HA-Ty hydrogel has emerged as a highly potent and advanced wound healing material.

Declaration of competing interest

The author declares no conflict of interest, financial or otherwise.

Acknowledgements

This research did not receive any specific grant from funding agencies in the public, commercial, or not-for-profit sectors. The authors are helpful to the National Institute of Technology (NIT), Rourkela, Odisha, India for providing all required facilities. The authors would also like to thank to Columbia Institute of Pharmacy, Raipur, Chhattisgarh, India for providing laboratory animal facilities.

References

1. J. Koehler, F.P. Brandl, A.M. Goepferich, Hydrogel wound dressings for bioactive treatment of acute and chronic wounds, Eur. Polym. J. 100

Journal of Chemical Health Risks

www.jchr.org

JCHR (2023) 13(6), 2569-2588 | ISSN:2251-6727

(2018) 1–11, doi:10.1016/j.eurpolymj.2017.12.046.

2. A.Ghahary, A. Ghaffari, Role of keratinocyte–fibroblast cross-talk in development of hypertrophic scar, Wound Repair Regener. 15 (s1) (2007) S46–S53, doi:10.1111/j.1524-475X.2007.00225.x.
3. R. Li, K. Liu, X. Huang, D. Li, J. Ding, B. Liu, X. Chen, Bioactive materials promote wound healing through modulation of cell behaviors, Adv. Sci. 9 (10) (2022) 2105152, doi:10.1002/advs.202105152
4. A.Benedetto, J. Staidle, J. Schoenfeld, E. Benedetto, P. Benedetto, Comparing the use of a novel antibiotic-free film-forming topical wound dressing *versus* a topical triple antibiotic in dermatologic surgical procedures including Mohs micrographic surgery, J. Eur. Acad. Dermatol. Venereol. 35 (1) (2021) 247–255, doi:10.1111/jdv.16965.
5. S. Atta, S. Khaliq, A. Islam, I. Javeria, T. Jamil, M.M. Athar, M.I. Shafiq, A. Ghaffar, Injectable biopolymer based hydrogels for drug delivery applications, Int. J. Biol. Macromol. 80 (2015) 240–245, doi:10.1016/j.ijbiomac.2015.06.044.
6. B.O. Okesola, S. Ni, B. Derkus, C.C. Galeano, A. Hasan, Y. Wu, J. Ramis, L. Buttery, J.I. Dawson, M. D'Este, Growth-factor free multicomponent nanocomposite hydrogels that stimulate bone formation, Adv. Funct. Mater. 30 (14) (2020) 1906205, doi:10.1002/adfm.201906205.
7. R. Xing, K. Liu, T. Jiao, N. Zhang, K. Ma, R. Zhang, Q. Zou, G. Ma, X. Yan, An injectable self-assembling collagen–gold hybrid hydrogel for combinatorial antitumor photothermal/photodynamic therapy, Adv. Mater. 28 (19) (2016) 3669– 3676, doi:10.1002/adma.201600284.
8. J.A. Burdick, G.D. Prestwich, Hyaluronic acid hydrogels for biomedical applications, Adv. Mater. 23 (12) (2011) H41–H56, doi:10.1002/adma.201003963.
9. K.Y. Choi, H.S. Han, E.S. Lee, J.M. Shin, B.D. Almquist, D.S. Lee, J.H. Park, Hyaluronic acid–based activatable nanomaterials for stimuli-responsive imaging and therapeutics: beyond CD44-mediated drug delivery, Adv. Mater. 31 (34) (2019) 1803549, doi:10.1002/adma.201803549.
10. R.R. Chen, D.J. Mooney, Polymeric growth factor delivery strategies for tissue engineering, Pharm. Res. 20 (2003) 1103–1112, doi:10.1023/a:1025034925152.
11. M.E. Klontzas, S. Reakasame, R. Silva, J.C. Morais, S. Vernardis, R.J. MacFarlane, M. Heliotis, E. Tsiridis, N. Panoskaltsis, A.R. Boccaccini, Oxidized alginate hydrogels with the GHK peptide enhance cord blood mesenchymal stem cell osteogenesis: a paradigm for metabolomics-based evaluation of biomaterial design, ActaBiomater. 88 (2019) 224–240, doi:10.1016/j.actbio.2019.02.017.
12. C. Conato, R. Gavioli, R. Guerrini, H. Kozłowski, P. Młynarz, C. Pasti, F. Pulidori, M. Remelli, Copper complexes of glycyl-histidyl-lysine and two of its synthetic analogues: chemical behaviourand biological activity, Biochim. Biophys. Acta 1526 (2) (2001) 199–210, doi:10.1016/S0304-4165(01)00127-1.
13. Y.M. Abul-Haija, G.G. Scott, J.K. Sahoo, T. Tuttle, R.V. Ulijn, Cooperative, ionsensitive co-assembly of tripeptide hydrogels, Chem. Commun. 53 (69) (2017) 9562–9565, doi:10.1039/c7cc04796g.
14. Y. Li, X. Cai, Z. Wang, Y. Han, C. Ren, L. Yang, Z. Wang, G. Mu, H. Jia, J. Liu, J. Liu, C. Yang, Bio-inspired supramolecularmetallopeptide hydrogel promotes recovery from cutaneous wound, Chem. Eng. J. 455 (2023) 140848, doi:10. 1016/j.cej.2022.140848.
15. M. Plätzer, J. Ozegowski, R. Neubert, Quantification of hyaluronan in pharmaceutical formulations using high performance capillary electrophoresis and the modified uronic acid carbazole reaction, J. Pharm. Biomed. Anal. 21 (3) (1999) 491–496, doi:10.1016/S0731-7085(99)00120-X.
16. A.Saiga, S. Tanabe, T. Nishimura, Antioxidant activity of peptides obtainedfrom porcine myofibrillar proteins by protease treatment, J. Agric. Food Chem. 51 (12) (2003) 3661–3667, doi:10.1021/jf021156g.
17. C.M. Elvin, A.G. Carr, M.G. Huson, J.M. Maxwell, R.D. Pearson, T. Vuocolo, N.E.

Journal of Chemical Health Risks

www.jchr.org

JCHR (2023) 13(6), 2569-2588 | ISSN:2251-6727

Liyou, D.C.C. Wong, D.J. Merritt, N.E. Dixon, Synthesis and properties of crosslinked recombinant pro-resilin, Nature 437 (7061) (2005) 999–1002, doi:10.1038/nature04085.

18. A.M. Aviv, M. Halperin-Sternfeld, I. Grigoriants, L. Buzhansky, I. Mironi-Harpaz, D. Seliktar, S. Einav, Z. Nevo, L. Adler-Abramovich, Improving the mechanical rigidity of hyaluronic acid by integration of a supramolecular peptide matrix, ACS Appl. Mater. Interfaces 10 (49) (2018) 41883–41891, doi:10.1021/acsami.8b08423.
19. A.Gruchlik, M. Jurzak, E. Chodurek, Z. Dzierzewicz, Effect of Gly-Gly-His, Gly-His-Lys and their copper complexes on TNF-alpha-dependent IL-6 secretion in normal human dermal fibroblasts, Acta Pol. Pharm. 69 (6) (2012) 1303–1306.
20. A.Senturk, S. Mercan, T. Delibasi, M.O. Guler, A.B. Tekinay, Angiogenic peptide nanofibers improve wound healing in STZ-induced diabetic rats, ACS Biomater. Sci. Eng. 2 (7) (2016) 1180–1189, doi:10.1021/acsbiomaterials.6b00238.
21. Y. Sun, C. Kang, Z. Yao, F. Liu, Y. Zhou, Peptide-based ligand for active delivery of liposomal doxorubicin, Nano Life 06 (03n04) (2016) 1642004, doi:10.1142/s1793984416420046.
22. M. Delfi, R. Sartorius, M. Ashrafizadeh, E. Sharifi, Y. Zhang, P. De Berardinis, A. Zarrabi, R.S. Varma, F.R. Tay, B.R. Smith, P. Makvandi, Self-assembled peptide and protein nanostructures for anti-cancer therapy: targeted delivery, stimuli-responsive devices and immunotherapy, Nano Today 38 (2021) 101119, doi:10.1016/j.nantod.2021.101119.
23. F. Pereira Beserra, M. Xue, G.L.A. Maia, A. Leite Rozza, C. Helena Pellizzon, C.J. Jackson, Lupeol, a pentacyclic triterpene, promotes migration, wound closure, and contractile effect in vitro: possible involvement of PI3K/Akt and p38/ERK/MAPK pathways, Molecules 23 (11) (2018), doi:10. 3390/molecules23112819.
24. X. He, Y. Li, B. Deng, A. Lin, G. Zhang, M. Ma, Y. Wang, Y. Yang, X. Kang, The PI3K/AKT signalling pathway in inflammation, cell death and glial scar formation after traumatic spinal cord injury: mechanisms and therapeutic opportunities, Cell Prolif. 55 (9) (2022) e13275, doi:10.1111/cpr.13275.
25. S.R. Bolla, A. Mohammed Al-Subaie, R. Yousuf Al-Jindan, J. PapayyaBalakrishna, P. Kanchi Ravi, V.P. Veeraraghavan, A. Arumugam Pillai, S.S.R. Gollapalli, J. Palpath Joseph, K.M. Surapaneni, *In vitro* wound healing potency of methanolic leaf extract of Aristolochiasaccata is possibly mediated by its stimulatory effect on collagen-1 expression, Heliyon 5 (5) (2019) e01648, doi:10.1016/j.heliyon.2019.e01648.
26. X. Ren, Y. Han, J. Wang, Y. Jiang, Z. Yi, H. Xu, Q. Ke, An aligned porous electrospun fibrous membrane with controlled drug delivery - An efficient strategy to accelerate diabetic wound healing with improved angiogenesis, ActaBiomater. 70 (2018) 140–153, doi:10.1016/j.actbio.2018.02.010.
27. P. Victor, D. Sarada, K.M. Ramkumar, Pharmacological activation of Nrf2 promotes wound healing, Eur. J. Pharmacol. 886 (2020) 173395, doi:10.1016/j.ejphar.2020.173395
28. J.F. Luo, X.Y. Shen, C.K. Lio, Y. Dai, C.S. Cheng, J.X. Liu, Y.D. Yao, Y. Yu, Y. Xie, P. Luo, X.S. Yao, Z.Q. Liu, H. Zhou, Activation of Nrf2/HO-1 pathway by nardochinoid C inhibits inflammation and oxidative stress in lipopolysaccharidestimulated macrophages, Front. Pharmacol. 9 (2018) 911, doi:10.3389/fphar.2018.00911.
29. N. Ganapathy, S.S. Venkataraman, R. Daniel, R.J. Aravind, V.B. Kumarakrishnan, Molecular biology of wound healing, J. Pharm. Bioallied Sci. 4 (Suppl 2) (2012) S334–S337, doi:10.4103/0975-7406.100294.
30. A.W. James, G. LaChaud, J. Shen, G. Asatrian, V. Nguyen, X. Zhang, K. Ting, C. Soo, A review of the clinical side effects of bone morphogenetic protein-2, Tissue Eng. Part B 22 (4) (2016) 284–297, doi:10.1089/ten.TEB.2015.0357.
31. S. Trujillo, C. Gonzalez-Garcia, P. Rico, A. Reid, J. Windmill, M.J. Dalby, M. Salmeron-Sanchez, Engineered 3D hydrogels with full-length fibronectin that sequester and present growth factors, Biomaterials 252 (2020) 120104,

Journal of Chemical Health Risks

www.jchr.org

JCHR (2023) 13(6), 2569-2588 | ISSN:2251-6727

doi:10.1016/j.biomaterials.2020.120104.

32. B. Latha, R. Likhitha, C. Kumar, Copper chelating protein hydrolysate from Salvia hispanica L. by pepsin-pancreatin treatment, Curr. Res. Food Sci. 4 (2021) 829–839, doi:10.1007/s00217-009-1178-x.
33. E.C. Wu, S. Zhang, C.A.E. Hauser, Self-assembling peptides as cell-interactive scaffolds, Adv. Funct. Mater. 22 (3) (2012) 456–468, doi:10.1002/adfm.201101905.
34. K. Strauss, J. Chmielewski, Advances in the design and higher-order assembly of collagen mimetic peptides for regenerative medicine, Curr. Opin. Biotechnol. 46 (2017) 34–41, doi:10.1016/j.copbio.2016.10.013.
35. B. Senturk, S. Mercan, T. Delibasi, M.O. Guler, A.B. Tekinay, Angiogenic peptide nanofibers improve wound healing in STZ-induced diabetic rats, ACS Biomater. Sci. Eng. 2 (7) (2016) 1180–1189, doi:10.1021/acsbiomaterials.6b00238.
36. N. Habibi, N. Kamaly, A. Memic, H. Shafiee, Self-assembled peptide-based nanostructures: smart nanomaterials toward targeted drug delivery, Nano Today 11 (1) (2016) 41–60, doi:10.1016/j.nantod.2016.02.004.
37. X.J. Wang, J. Cheng, L.Y. Zhang, J.G. Zhang, Self-assembling peptides-based nano-cargos for targeted chemotherapy and immunotherapy of tumors: recent developments, challenges, and future perspectives, Drug Deliv. 29 (1) (2022) 1184–1200, doi:10.1080/10717544.2022.2058647.
38. J.Z. Du, T.M. Sun, W.J. Song, J. Wu, J. Wang, A tumor-acidity-activated chargeconversionalnanogel as an intelligent vehicle for promoted tumoral-cell uptake and drug delivery, Angew. Chem. Int. Ed. Engl. 49 (21) (2010) 3621–3626, doi:10.1002/anie.200907210.
39. Y. Sun, C. Kang, Z. Yao, F. Liu, Y. Zhou, Peptide-based ligand for active delivery of liposomal doxorubicin, Nano Life 06 (03n04) (2016) 1642004, doi:10.1142/s1793984416420046.
40. V. Castelletto, I.W. Hamley, C. Whitehouse, P.J. Matts, R. Osborne, E.S. Baker, Self-assembly of palmitoyl lipopeptides used in skin care products, Langmuir 29 (29) (2013) 9149–9155, doi:10.1021/la401771j.